Pergamon

Int. J. Solids Structures Vol 31, No. 8, pp. 1047–1061, 1994

0020–7683/94 $6.00 + .00

A COUPLED FE AND BOUNDARY INTEGRAL EQUATION METHOD BASED ON EXTERIOR DOMAIN DECOMPOSITION FOR FLUID–STRUCTURE INTERFACE PROBLEMS

XIAOGANG ZENG and FANG ZHAO†
Department of Civil and Environmental Engineering, Florida International University, Miami, FL 33199, U.S.A.

(*Received* 19 *July* 1993 ; *in revised form* 7 *October* 1993)

Abstract—A coupled finite element and exterior domain decomposition-based boundary integral formulations for the solutions of two- or three-dimensional time-harmonic fluid–structure interaction problems is described in this paper. It is known that the memory limitation of computers has been one of the major obstacles for solving large scale high frequency fluid–structure interface systems using various existing nonlocal finite element and boundary integral equation coupling techniques due to the fully populated resultant matrix generated from the boundary integral equation representation. The essence of this study is to decompose, through domain decomposition of the exterior region, the original exterior problem into arbitrary subproblems with data sharing only at the interfaces. By decomposing the exterior infinite domain into an appropriate number of infinite subdomains, this method not only ensures the validity of the formulation for all frequencies but also leads to a diagonalized, blockwise-banded system of discretized equations. The size of an individual submatrix (i.e. a block) that is associated with an exterior subdomain may be decided by the user, and may be selected such that the restriction due to the memory limitation of a given computer may be accommodated. In addition, the method is suited for parallel processing since the data associated with each subdomain (impedance matrices, load vectors, etc.) may be generated in parallel, and the communication needed will be only for the interface values. Most significantly, unlike the existing coupled finite element and boundary integral equation techniques that are valid for all frequencies, our method avoids the use of both the hypersingular operator and the double integrals, therefore reducing the computational complexity. Numerical experiments have been performed for elastic cylindrical shells subjected to a plane incident wave. The results have demonstrated the accuracy of the method for wavenumbers ranging from 0 to 30, both directly on the shell and in the far field, and have confirmed that the procedure is valid for all frequencies.

1. INTRODUCTION

In this paper we are concerned with the problem of scattering by a deformable obstacle in an acoustic medium, and its solution via a coupled finite element (FE) and exterior domain decomposition (DD) based boundary integral equation (BIE) method, which is intended as a prototype for a class of more general scattering and radiation problems that occur in such diverse fields as elastodynamics and electromagnetism.

Various coupled FE and BIE methods have been widely used for studying problems of wave scattering by deformable structures submerged in a compressible, inviscid fluid. The interior structures, due to their complex structural or geometrical configurations, which may include, for example, inhomogeneous or nonlinear elastic solids, plate, shell, etc., or their combinations, are usually represented using FE techniques, while the exterior fluid media are formulated by BIE methods because of their ability to reduce by one the dimension of the subproblem associated with the exterior region, as well as the added attraction of automatically satisfying the appropriate radiation conditions. Some recent work in using the coupled FE and BIE methods to solve wave scattering problems may be found among others, in Chien *et al.* (1990), Ginsberg *et al.* (1990), Jeans and Mathews (1990), Kallivokas *et al.* (1993), Krishnasamy *et al.* (1990), Seybert *et al.* (1985, 1988) and Zeng *et al.* (1992a–c).

In the existing coupled FE and BIE methods, one of the drawbacks of using BIE methods to represent the exterior region is that, contrary to interior FE formulations, which upon discretization lead to large but sparse algebraic systems, BIE formulations give rise

† To whom correspondence should be addressed.

to smaller but full systems of equations. Thus, the resultant coupled FE and BIE system loses the sparseness of the matrix stemming from the interior structure that is usually responsible for the majority of the unknowns in the final system of equations. The nonlocality of the coupled FE and BIE methods makes their use difficult in practice for problems that involve radiating or scattering structures if the wavelength of the excitation is small compared to the largest dimension of the structure, even with the largest computers now available. This difficulty has been addressed in the domain finite element and finite difference communities by developing infinite elements (Zienkiewicz *et al.*, 1985) and artificial absorbing boundaries (Givoli, 1991). There has also been some effort to overcome this difficulty with boundary elements through localization. In the early 1980s, Kagawa *et al.* (1983) developed an infinite boundary element technique for two-dimensional problems that produces sparse impedance matrices, but due perhaps to the somewhat *ad hoc* procedure used in their derivation, such infinite elements have not been adopted in practice. Another drawback of some of the existing coupled FE and BIE techniques is that they suffer from the nonuniqueness or nonexistence of solutions at the characteristic frequencies of the associated interior problems. This problem is due to the failure of the boundary integral representation of domain governing conditions. In the coupled FE and BIE method, the governing equation of the exterior medium is represented by a BIE defined on the interface. However, when the interface itself is a nodal line (or surface) of an eigenfunction of the integral operator, the operator becomes singular and thus fails to represent the exterior domain governing condition. Physically, this eigenfunction coincides with an eigenmode of a problem defined over the interior region with the same integral equation as its representation of the interior governing condition, but with different boundary conditions. This phenomenon is usually referred to, in the literature, as failure at the characteristic of the associated interior problems, and the corresponding frequency (wavenumber) of excitation is called critical or characteristic frequency (wavenumber) of the associated interior problems. It is obvious that the nonuniqueness or nonexistence of solutions for the coupled FE and BIE does not have any physical meaning ; it arises entirely from the failure of the boundary integral representation for the exterior problem at the frequencies that are characteristic of the associated interior problems. This failure of the exterior integral equations at the interior resonant frequencies was first noted by Lamb (1945), and then by Schenck (1968). Since then, various formulations and numerical techniques have been developed to circumvent this deficiency. Reviews on the various methods may be found, among others, in Zeng (1992) and Chien *et al.* (1990). More recently, two different, systematic variational BIE methods based on an exterior domain decomposition have been developed by Zeng *et al.* (1992a) and Zeng and Bielak (1992) for generating sparse, symmetric, impedance matrices. Both methods involve the use of double integrals, while the former also uses the normal derivative of the double-layer potential, i.e. a hypersingular operator, to derive a stable procedure that is valid for all frequencies. In this paper, we describe a new coupled FE and BIE method based on the domain decomposition of the exterior region in the spirit of Zeng *et al.* (1992a) and Zeng and Bielak (1992), in order to obtain a new sparse formulation that does not involve double integrals and the hypersingular operator and, therefore, results in reduced computational complexity. In the next section we describe the proposed methodology as it applies to three-dimensional fluid–structure interaction problems, but illustrate its applicability with numerical examples in two dimensions, for wavenumbers in the range of 0–30.

2. STATEMENT OF PROBLEM AND FORMULATION

Consider the geometry shown in Fig. 1. The region Ω in $\mathbf{R}^3$ with boundary Γ is occupied by a linear elastic scatterer with density ρ_e and Lamé material parameters μ_e and λ_e. The exterior region Ω_f represents a homogeneous, compressible, inviscid fluid with density ρ_f and speed of sound c_f. We assume that there is an incident steady-state harmonic fluid motion given by a pressure $P^0(\mathbf{x}, t) = \mathrm{Re}\,[p^0(\mathbf{x}) \exp(i\omega t)]$, where ω is the frequency of excitation. We denote the total pressure in the fluid by $Q(\mathbf{x}, t) = \mathrm{Re}\,[q(\mathbf{x}) \exp(i\omega t)]$, the scattered pressure by $P(\mathbf{x}, t) = \mathrm{Re}\,[p(\mathbf{x}) \exp(i\omega t)] = Q - P^0$, and use $\mathbf{U}(\mathbf{x}, t) = \mathrm{Re}\,[\mathbf{u}(\mathbf{x})$

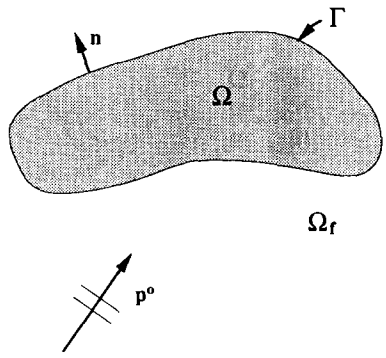

Fig. 1. Elastic obstacle immersed in a compressible, inviscid fluid.

$\exp(i\omega t)]$ and $\mathbf{\Sigma}[\mathbf{U}] = \mu_e[\nabla\mathbf{U} + (\nabla\mathbf{U})^T] + \lambda_e(\nabla\cdot\mathbf{U})\mathbf{I}$ to represent, respectively, the displacement and the stress fields in the interior structure. The fluid–structure interaction problem then consists in finding $\mathbf{u}$ and p such that :

$$\nabla^2 p + k_f^2 p = 0, \quad k_f^2 \equiv \omega^2/c_f^2, \quad \text{in } \Omega_f, \tag{1a}$$

$$\nabla\cdot\boldsymbol{\sigma}[\mathbf{u}] + \rho_e\omega^2\mathbf{u} = 0, \quad \text{in } \Omega, \tag{1b}$$

$$\sigma_{nn} \equiv \boldsymbol{\sigma}[\mathbf{u}] : \mathbf{nn} = -(p+p^0), \qquad \sigma_{n\tau} \equiv \boldsymbol{\sigma}[\mathbf{u}] : \mathbf{n}\boldsymbol{\tau} = 0, \quad \text{on } \Gamma \tag{1c, d}$$

$$u_n \equiv \mathbf{u}\cdot\mathbf{n} = \frac{1}{\rho_f\omega^2}(p_n + p_n^0), \quad \text{on } \Gamma \tag{1e}$$

$$p \text{ satisfies a radiation condition in } \Omega_f, \tag{1f}$$

where $\boldsymbol{\sigma}[\mathbf{u}] \equiv \mu_e[\nabla\mathbf{u} + (\nabla\mathbf{u})^T] + \lambda_e(\nabla\cdot\mathbf{u})\mathbf{I}$, $\mathbf{n}$ and $\boldsymbol{\tau}$ are, respectively, the outward normal and tangential unit vectors (cf. Fig. 1), and the subscript n in p_n and p_n^0 denotes normal derivative. Equations (1a) and (1b) are, respectively, the steady-state equations of motion for the exterior fluid and the interior elastic solid, while eqns (1c, d) and (1e) represent, respectively, the normal, the tangential traction and the displacement transition conditions on the fluid–solid interface Γ.

In order to subsequently solve this problem, we decompose the exterior region Ω_f into M subdomains Ω^i, $i = 1, 2, \ldots, M$, with Γ^i denoting the boundary of Ω^i, and Γ_0^i the part of the interface Γ common to Γ^i, i.e. $\Gamma_0^i \equiv \Gamma_i \cap \Gamma$, as shown in Fig. 2. By renaming p and p_{n_i} within Ω^i as $\phi^{(i)}$ and $\psi^{(i)}$, respectively, eqn (1) may then be rewritten as follows :

$$\nabla^2\phi^{(i)} + k_f^2\phi^{(i)} = 0, \quad \text{in } \Omega^i, \quad i = 1, 2, \ldots, M, \tag{2a}$$

$$\nabla\cdot\boldsymbol{\sigma}[\mathbf{u}] + \rho_e\omega^2\mathbf{u} = 0, \quad \text{in } \Omega, \tag{2b}$$

$$\phi^{(i)} = \phi^{(j)}, \qquad \psi^{(i)} = -\psi^{(j)}, \quad \text{on } \Gamma^{ij} \equiv \Gamma^i \cap \Gamma^j, \tag{2c, d}$$

$$\sigma_{nn} \equiv \boldsymbol{\sigma}[\mathbf{u}] : \mathbf{nn} = -(\phi^{(i)} + p^0), \qquad \sigma_{n\tau} \equiv \boldsymbol{\sigma}[\mathbf{u}] : \mathbf{n}\boldsymbol{\tau} = 0, \quad \text{on } \Gamma_0^i, \tag{2e, f}$$

$$u_{n_i} \equiv \mathbf{u}\cdot\mathbf{n}_i = -\frac{1}{\rho_f\omega^2}(p_n + p_n^0) = \frac{1}{\rho_f\omega^2}(\psi^i + p_{n_i}^0), \quad \text{on } \Gamma_0^i, \quad i = 1, 2, \ldots, M, \tag{2g}$$

$$\phi^{(i)} \text{ satisfies a radiation condition in } \Omega^i, \quad i = 1, 2, \ldots, M. \tag{2h}$$

Equations (2b) and (2e, f) represent the governing conditions for the interior structure that will be formulated with standard FE techniques. From the FE theory, the total energy functional of the interior problem may be written as

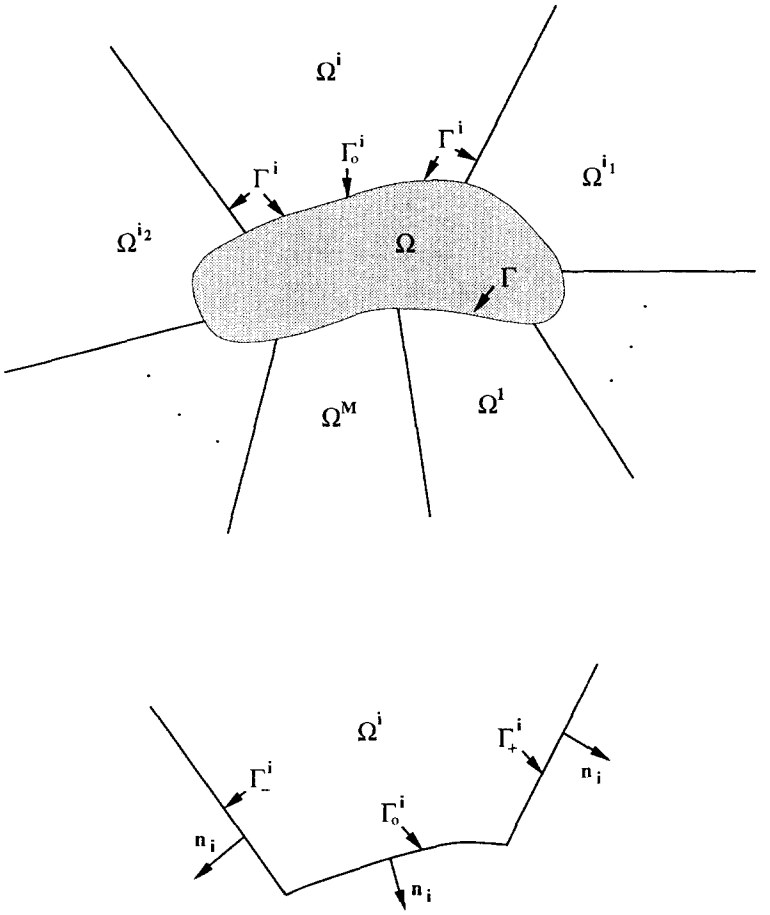

Fig. 2. Obstacle and fluid, showing partitioning into macro-elements and a typical exterior macro-element.

$$\Pi(\mathbf{u}) = \frac{1}{2}\int_\Omega (\boldsymbol{\sigma}[\mathbf{u}] : \nabla\mathbf{u} - \rho_e\omega^2\mathbf{u}^2)\,d\Omega + \sum_{i=1}^{M}\left[\int_{\Gamma_0^i}(p^0+\phi^{(i)})u_{n_i}\,d\Gamma_0^i\right], \tag{3}$$

where the unknown boundary pressure $\phi^{(i)}$ is considered as a parameter that will be determined from the exterior governing conditions (2a) and (2h). It is easy to verify that by setting the first variation $\delta\Pi$ to vanish, i.e. $\delta\Pi = 0$, for an arbitrary variation $\delta\mathbf{u}$ and considering the unknown pressure $\phi^{(i)}$ as a parameter will lead to the governing conditions (2b) and (2e, f) for the interior structure.

To determine the unknown pressure $\phi^{(i)}$ and to ensure that $\phi^{(i)}$ satisfies (2a) and (2h), we make use of the Helmholtz representation formula:

$$\phi^{(i)} = \mathscr{D}^{(i)}[\phi^{(i)}] - \mathscr{S}^{(i)}[\psi^{(i)}], \quad \text{in } \Omega^i, \tag{4}$$

in which $\mathscr{S}^{(i)}$ and $\mathscr{D}^{(i)}$ are the single- and double-layers:

$$\mathscr{S}^{(i)}[\chi](\mathbf{x}) \equiv \int_{\Gamma^i}\chi(\mathbf{y})G(|\mathbf{x}-\mathbf{y}|)\,d\Gamma^i(\mathbf{y}), \tag{5a}$$

$$\mathscr{D}^{(i)}[\chi](\mathbf{x}) \equiv \int_{\Gamma^i}\chi(\mathbf{y})\frac{\partial}{\partial n(\mathbf{y})}G(|\mathbf{x}-\mathbf{y}|)\,d\Gamma^i(\mathbf{y}), \tag{5b}$$

and $G(z)$ is the fundamental singularity, or Green's function, for (2a, h):

$$G(z) \equiv -\frac{1}{4\pi z}\exp(ikz), \quad \text{in } \mathbf{R}^3, \quad G(z) \equiv \frac{i}{4}H_0^{(2)}(ikz), \quad \text{in } \mathbf{R}^2. \tag{6a, b}$$

Thus, $\phi^{(i)}$ in (4) automatically satisfies (2a) and (2h) for arbitrary $\phi^{(i)}$ and $\psi^{(i)}$. For smooth χ and Γ^i one has the jump relations :

$$\mathscr{S}^{(i)}[\chi]^- = S^{(i)}[\chi], \qquad \mathscr{D}^{(i)}[\chi]^- = \tfrac{1}{2}\chi + D^{(i)}[\chi], \tag{7a, b}$$

where the minus sign denotes the limit on Γ^i from Ω^i. Boundary integral methods based on the Helmholtz representation formula (4) are usually referred to as *direct* since the pressure $\phi^{(i)}$ at any point within the fluid is expressed directly in terms of the physical quantities $\phi^{(i)}$ and $\psi^{(i)}$ on the boundary. From the jump relations (7a, b) and (4), it follows that

$$\tfrac{1}{2}\phi^{(i)} - D^{(i)}[\phi^{(i)}] + S^{(i)}[\psi^{(i)}] = 0, \quad \text{on } \Gamma^i, \quad i = 1, 2, \ldots, M. \tag{8}$$

The boundary integral equation (8) and its corresponding continuity conditions (2c, d), and the transition condition (2g), as well as the interior governing conditions derived from the variational condition $\delta\Pi = 0$, are the basic relationships for the numerical implementation described in the next section.

Remarks

(i) The present method is valid for all frequencies. This follows directly from the fact that (8) has no critical frequencies since both Ω^i and its complementary domain are unbounded. It is thus clear that the idea of decomposing Ω_f into two or more unbounded subdomains, in addition to leading to a local formulation, makes the present method free from the usual defect associated with standard boundary integral formulations.

(ii) The system of algebraic equations obtained upon discretization of the unknowns $\phi^{(i)}$ and $\psi^{(i)}$ will be blockwise banded since, like the FE method, unknowns in one subdomain are coupled only with those of neighboring subdomains. The size of the submatrix (block) of each subdomain may be adjusted to meet the requirement of a particular computer architecture.

(iii) The present method promises various condensation schemes to obtain optimal numerical efficiency. Examples of such schemes include, for example, the condensation of $\psi^{(i)}$ in terms of $\phi^{(i)}$ and $\mathbf{u}$, or the condensation of both $\psi^{(i)}$ and $\mathbf{u}$ in terms of $\phi^{(i)}$. The procedures may be performed either sequentially or in parallel. The resultant system will be smaller yet still blockwise banded, thus promising a powerful numerical method for large scale high frequency fluid–structure interaction problems.

(iv) While the basic ideas behind the present exterior domain decomposition method come from Zeng *et al.* (1992a) and Zeng and Bielak (1992), the numerical implementation is much simpler due to the fact that there are no hypersingular operator and double integrals in this formulation. The price paid by using this simpler method is that the resultant system is no longer symmetric. Comparing with the coupled FE–BIE method in Zeng and Bielak (1992), which involves double integrals to construct the symmetric "effective stiffness" matrix, it seems that the present method requires more time to solve the resultant system of equations, while the variational principle-based FE–BIE method in Zeng and Bielak (1992) requires more time to construct the final system matrix. Limited numerical results have shown that the present method is faster than that in Zeng and Bielak (1992). However, the issues of numerical efficiency of coupling methods that are based on variational principles and on collocational methods need to be carefully investigated before any conclusions may be reached.

3. FINITE/BOUNDARY ELEMENT DISCRETIZATION

We consider here the numerical solution of the coupled problem described in eqns (2b, e, f), which represent the corresponding interior problem, and eqns (8) and (2c, d),

which represent the associated exterior problem, as well as the displacement transition condition (2g). To derive the matrix form governing equations of the coupled system, we first divide the boundary Γ^i of each subdomain Ω^i into three segments, i.e. $\Gamma^i = \Gamma^i_0 \cup \Gamma^i_+ \cup \Gamma^i_-$ (cf. Fig. 2), where Γ^i_+ and Γ^i_- represent, respectively, the two, i.e. the right and the left, ray boundary segments of the subdomain, while Γ^i_0 is the boundary portion that has a finite length. For conciseness, we also use the subscripts 0, − and + to denote variables that are defined on boundary segments Γ^i_0, Γ^i_+ and Γ^i_-, respectively.

For the interior structure, we use the standard FE discretization scheme. Detailed description of the FE procedures may be found, for instance, in Zeng (1992), Bathe (1982) or Hughes (1987). The total energy functional of the interior structure defined in (3) may be approximated as

$$\hat{\Pi}(\hat{\mathbf{u}}) = \tfrac{1}{2}\hat{\mathbf{u}}^T\mathbf{K}_{uu}\hat{\mathbf{u}} + \sum_{i=1}^{M}[(\hat{\mathbf{u}}_0^{(i)})^T\mathbf{K}^{(i)}_{u_0\phi_0}\hat{\boldsymbol{\phi}}_0^{(i)} + (\hat{\mathbf{u}}_0^{(i)})^T\mathbf{f}^{(i)}_{u_0}], \tag{9}$$

in which $\mathbf{K}_{uu}$ represents the standard impedance symmetric matrix of the interior structure, $\hat{\mathbf{u}}$ is the total nodal displacement vector of the system, $\hat{\mathbf{u}}_0^{(i)}$† and $\hat{\boldsymbol{\phi}}_0^{(i)}$ are, respectively, the nodal displacement and pressure vectors on Γ^i_0, $\mathbf{f}^{(i)}_{u_0}$ is the known nodal force vector on Γ^i_0, corresponding to the given incident wave p^0, and $\mathbf{K}^{(i)}_{u_0\phi_0}$ represents the coupling matrix of $\hat{\mathbf{u}}_0^{(i)}$ and $\hat{\boldsymbol{\phi}}_0^{(i)}$ on Γ^i_0.

To obtain the matrix form governing conditions for the interior problem, set the first variation of functional (9) to zero for an arbitrary variation $\delta\hat{\mathbf{u}}$ and consider $\hat{\boldsymbol{\phi}}_0^{(i)}$ on each Γ^i_0 as a parametric vector. This results in

$$(\delta\hat{\mathbf{u}})^T\mathbf{K}_{uu}\hat{\mathbf{u}} + \sum_{i=1}^{M}(\delta\hat{\mathbf{u}}_0^{(i)})^T(\mathbf{K}^{(i)}_{u_0\phi_0}\hat{\boldsymbol{\phi}}_0^{(i)} + \mathbf{f}^{(i)}_{u_0}) \equiv (\delta\hat{\mathbf{u}})^T(\mathbf{K}_{uu}\hat{\mathbf{u}} + \mathbf{K}_{u\phi_0}\hat{\boldsymbol{\phi}}_0 + \mathbf{f}_u) = 0, \tag{10}$$

which leads to a system of N_u linear algebraic equations for $\hat{\mathbf{u}}$,

$$\mathbf{K}_{uu}\hat{\mathbf{u}} + \mathbf{K}_{u\phi_0}\hat{\boldsymbol{\phi}}_0 + \mathbf{f}_u = 0, \tag{11}$$

where N_u is the number of the total displacement unknowns of the interior structure and $\hat{\boldsymbol{\phi}}_0$ represents the nodal point vector for pressure ϕ on the interface Γ. The linear system of equations (11) consists of N_u equations with $N_u + N_{\phi_0}$ unknown variables, where N_{ϕ_0} denotes the total number of unknown nodal pressure in $\hat{\boldsymbol{\phi}}_0$. From the functional expression (3), it is easy to see that both $\mathbf{K}_{uu}$ and $\mathbf{K}_{u\phi_0}$ are banded matrices since the displacement and pressure, i.e. $\mathbf{u}$ and ϕ, in each element communicated only with those of its neighboring elements.

Since the system of linear equations (11) contains N_u equations with $N_u + N_{\phi_0}$ unknowns, additional equations must be obtained from the exterior governing conditions in order to solve the system. To derive these additional equations, we divide the boundary Γ^i of each subdomain $\Omega^{(i)}$ into boundary elements (cf. Fig. 3) and let the governing integral equation (8) be satisfied at nodal points,‡

$$\tfrac{1}{2}\phi_k^{(i)} - D^{(i)}[\phi_k^{(i)}] + S^{(i)}[\psi_k^{(i)}] = 0, \quad k = 1, 2, \ldots, K_i, \quad i = 1, 2, \ldots, M, \tag{12}$$

where k represents the individual nodal point while K_i is the total number of nodal points on Γ^i. Since $\phi^{(i)}$ and $\phi^{(j)}$ must be continuous at the interface $\Gamma^{ij} \equiv \Gamma^i \cap \Gamma^j$, we select a single mesh for this interface and approximate $\phi^{(i)}$ and $\phi^{(j)}$ on Γ^{ij} by identical interpolating functions defined by their nodal values. This ensures that ϕ will be continuous across the interfaces. For simplicity, in our numerical scheme, the pressure derivatives, transition

† The boundary nodal displacement vectors $\hat{\mathbf{u}}_0^{(i)}$, $i = 1, 2, \ldots, M$, are subsets of the total nodal displacement vector $\hat{\mathbf{u}}$.

‡ For a corner point, the factor $\frac{1}{2}$ becomes $\alpha/2\pi$, where α is the inner angle between the two boundary sections.

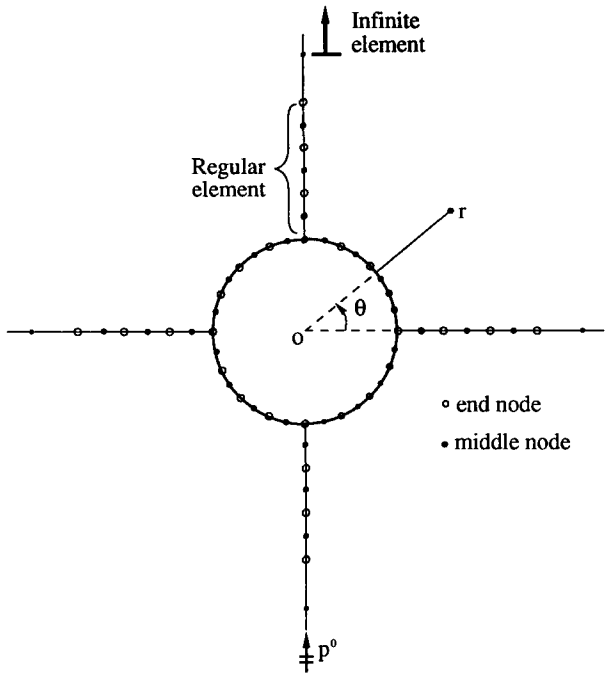

Fig. 3. Boundary element mesh for a circular cylindrical shell (four macro-elements each comprised of three regular elements and an infinite element on each ray and four regular elements on the arc).

conditions (2d) and the displacement transition condition (2g) are also satisfied by using identical shape functions (or elements) with the corresponding nodal point values satisfying

$$\psi_k^{(i)} + \psi_k^{(j)} = 0, \quad \text{on } \Gamma^{ij}, \tag{13}$$

and

$$\psi_k^{(i)} = \frac{1}{\rho_f \omega^2} u_{kn_i} - p^0_{kn_i}, \quad \text{on } \Gamma'_0 \equiv \Gamma \cap \Gamma', \quad i = 1, 2, \ldots, M. \tag{14}$$

It is easy to verify that eqns (12)–(14) and the interior eqns (11) give a sufficient number of equations to determine all the $\mathbf{u}$, ϕ and ψ unknown variables. However, for high frequency large scale fluid–structure interface problems, it may be more efficient or even inevitable to condense either ψ alone or both ψ and $\mathbf{u}$ to obtain a smaller yet still blockwise-banded system of linear equations.

On Γ^i, $\phi^{(i)}$ and $\psi^{(i)}$ may be approximated, in general, by standard boundary elements. The shape functions for $\phi^{(i)}$ and $\psi^{(i)}$ may be either constant, linear or quadratic. In this study, we use a quadratic shape function that corresponds to a three-mode element shown in Fig. 3 to interpolate all the variables. Special treatment, however, is required in order to represent these functions on Γ^{ij} due to the infinite extent of these interfaces. The procedure consists of introducing a strip of standard elements on each interface Γ^{ij} up to a certain distance away from Γ, and then using the mapped infinite elements developed originally for field equations by Zienkiewicz *et al.* (1985) to extend the solution to infinity. A detailed description of these infinite elements, which are based on assumed approximating functions that vary harmonically with kr and decay asymptotically as $1/kr$ and $1/\sqrt{kr}$ in three and two dimensions, is given therein, and an account of how they apply to the boundary integral approach may be found in Zeng *et al.* (1992a).

To illustrate the condensation and the solution scheme of the discretized system, it is convenient to consider two-dimensional scattering problems.† Consider a typical sub-domain Ω^i, shown in Fig. 2, where Γ^i_0, Γ^i_+ and Γ^i_- denote its three boundary segments.

† The three-dimensional case is similar but the numbering scheme is more cumbersome.

Equation (12) may be then rewritten as follows:

$$\tfrac{1}{2}\phi_k^{(i)} - D^{(i)}[\phi_k^{(i)}] + S_0^{(i)}[\psi_k^{(i)}] + S_+^{(i)}[\psi_k^{(i)}] + S_-^{(i)}[\psi_k^{(i)}] = 0, \quad k = 1, 2, \ldots, K_i, \tag{15}$$

where

$$S_0^{(i)}[\psi_k^{(i)}] \equiv \int_{\Gamma_0^i} G(|\mathbf{x}_k - \mathbf{y}|)\psi(\mathbf{y})\, d\Gamma_0^i(\mathbf{y}) \tag{16a}$$

$$S_\pm^{(i)}[\psi_k^{(i)}] \equiv \int_{\Gamma_\pm^i} G(|\mathbf{x}_k - \mathbf{y}|)\psi(\mathbf{y})\, d\Gamma_\pm^i(\mathbf{y}) \tag{16b}$$

$$D^{(i)}[\phi_k^{(i)}] \equiv \int_{\Gamma^i} \phi(\mathbf{y}) \frac{\partial}{\partial n(\mathbf{y})} G(|\mathbf{x}_k - \mathbf{y}|)\, d\Gamma^i(\mathbf{y}) \tag{16c}$$

and

$$S^{(i)}[\psi_k^{(i)}] \equiv S_0^{(i)}[\psi_k^{(i)}] + S_+^{(i)}[\psi_k^{(i)}] + S_-^{(i)}[\psi_k^{(i)}].$$

In matrix form, eqns (15) may be expressed as

$$\begin{bmatrix} \mathbf{A}_{01}^{(i)} & \mathbf{A}_{02}^{(i)} & \mathbf{A}_{03}^{(i)} & \mathbf{A}_{04}^{(i)} \\ \mathbf{A}_{+1}^{(i)} & \mathbf{A}_{+2}^{(i)} & \mathbf{A}_{+3}^{(i)} & \mathbf{A}_{+4}^{(i)} \\ \mathbf{A}_{-1}^{(i)} & \mathbf{A}_{-2}^{(i)} & \mathbf{A}_{-3}^{(i)} & \mathbf{A}_{-4}^{(i)} \end{bmatrix} \begin{Bmatrix} \hat{\boldsymbol{\phi}}^{(i)} \\ \hat{\boldsymbol{\psi}}_0^{(i)} \\ \hat{\boldsymbol{\psi}}_+^{(i)} \\ \hat{\boldsymbol{\psi}}_-^{(i)} \end{Bmatrix} = 0, \quad i = 1, 2, \ldots, M, \tag{17}$$

in which the coefficient submatrices $\mathbf{A}_{0j}$, $\mathbf{A}_{+j}$ and $\mathbf{A}_{-j}$ are associated, respectively, with the nodal points that are located on Γ_0^i, Γ_+^i and Γ_-^i. $\hat{\boldsymbol{\phi}}^{(i)}$ is the nodal point value vector of ϕ on Γ^i, whereas $\hat{\boldsymbol{\psi}}_0^{(i)}$, $\hat{\boldsymbol{\psi}}_+^{(i)}$ and $\hat{\boldsymbol{\psi}}_-^{(i)}$ are, respectively, the nodal point value vectors of ψ associated with the boundary segments Γ_0^i, Γ_+^i and Γ_-^i.

The condensation procedure may be described as follows. First, we rewrite the displacement transition condition (14) in matrix form:

$$\hat{\boldsymbol{\psi}}_0^{(i)} = \mathbf{A}_{\psi_0 u_0}^{(i)} \hat{\mathbf{u}}_0^{(i)} - \mathbf{f}_{p_{n_i}^0}, \quad i = 1, 2, \ldots, M. \tag{18}$$

By inserting (18) into (17), one eliminates the unknown vector $\hat{\boldsymbol{\psi}}_0^{(i)}$ and obtains

$$\begin{bmatrix} \mathbf{A}_{01}^{(i)} & \mathbf{B}_{02}^{(i)} & \mathbf{A}_{03}^{(i)} & \mathbf{A}_{04}^{(i)} \\ \mathbf{A}_{+1}^{(i)} & \mathbf{B}_{+2}^{(i)} & \mathbf{A}_{+3}^{(i)} & \mathbf{A}_{+4}^{(i)} \\ \mathbf{A}_{-1}^{(i)} & \mathbf{B}_{-2}^{(i)} & \mathbf{A}_{-3}^{(i)} & \mathbf{A}_{-4}^{(i)} \end{bmatrix} \begin{Bmatrix} \hat{\boldsymbol{\phi}}^{(i)} \\ \hat{\mathbf{u}}_0^{(i)} \\ \hat{\boldsymbol{\psi}}_+^{(i)} \\ \hat{\boldsymbol{\psi}}_-^{(i)} \end{Bmatrix} = \begin{Bmatrix} \mathbf{f}_0^{(i)} \\ \mathbf{f}_+^{(i)} \\ \mathbf{f}_-^{(i)} \end{Bmatrix}, \tag{19}$$

where

$$\mathbf{B}_{02}^{(i)} \equiv \mathbf{A}_{02}^{(i)} \mathbf{A}_{\psi_0 u_0}^{i}, \quad \mathbf{B}_{+2}^{(i)} \equiv \mathbf{A}_{+2}^{(i)} \mathbf{A}_{\psi_0 u_0}^{i}, \quad \mathbf{B}_{-2}^{(i)} \equiv \mathbf{A}_{-2}^{(i)} \mathbf{A}_{\psi_0 u_0}^{i},$$

and

$$\mathbf{f}_0^{(i)} \equiv \mathbf{A}_{02}^{(i)} \mathbf{f}_{p_{n_i}^0}, \quad \mathbf{f}_+^{(i)} \equiv \mathbf{A}_{+2}^{(i)} \mathbf{f}_{p_{n_i}^0}, \quad \mathbf{f}_-^{(i)} \equiv \mathbf{A}_{-2}^{(i)} \mathbf{f}_{p_{n_i}^0}.$$

To further eliminate vectors $\hat{\boldsymbol{\psi}}_+^{(i)}$ and $\hat{\boldsymbol{\psi}}_-^{(i)}$, we partition the matrix equation (19) into two sub-systems of equations:

$$\begin{bmatrix} \mathbf{A}_{+1}^{(i)} & \mathbf{B}_{+2}^{(i)} \\ \mathbf{A}_{-1}^{(i)} & \mathbf{B}_{-2}^{(i)} \end{bmatrix} \begin{Bmatrix} \hat{\boldsymbol{\phi}}^{(i)} \\ \hat{\mathbf{u}}_0^{(i)} \end{Bmatrix} + \begin{bmatrix} \mathbf{A}_{+3}^{(i)} & \mathbf{A}_{+4}^{(i)} \\ \mathbf{A}_{-3}^{(i)} & \mathbf{A}_{-4}^{(i)} \end{bmatrix} \begin{Bmatrix} \hat{\boldsymbol{\psi}}_+^{(i)} \\ \hat{\boldsymbol{\psi}}_-^{(i)} \end{Bmatrix} = \begin{Bmatrix} \mathbf{f}_+^{(i)} \\ \mathbf{f}_-^{(i)} \end{Bmatrix} \tag{20a}$$

and

$$[\mathbf{A}_{01}^{(i)} \quad \mathbf{B}_{02}^{(i)}]\begin{Bmatrix}\hat{\boldsymbol{\phi}}^{(i)}\\ \hat{\mathbf{u}}_0^{(i)}\end{Bmatrix}+[\mathbf{A}_{03}^{(i)} \quad \mathbf{A}_{04}^{(i)}]\begin{Bmatrix}\hat{\boldsymbol{\psi}}_+^{(i)}\\ \hat{\boldsymbol{\psi}}_-^{(i)}\end{Bmatrix}=\{\mathbf{f}_0^{(i)}\}. \tag{20b}$$

From eqn (20a), one can solve for $[\hat{\boldsymbol{\psi}}_+^{(i)}, \hat{\boldsymbol{\psi}}_-^{(i)}]^T$ in terms of $\hat{\boldsymbol{\phi}}^{(i)}$ and $\hat{\mathbf{u}}_0^{(i)}$ to obtain

$$\begin{Bmatrix}\hat{\boldsymbol{\psi}}_+^{(i)}\\ \hat{\boldsymbol{\psi}}_-^{(i)}\end{Bmatrix}\equiv\begin{Bmatrix}\mathbf{q}_+^{(i)}\\ \mathbf{q}_-^{(i)}\end{Bmatrix}-\begin{bmatrix}\mathbf{K}_{+\phi}^{(i)} & \mathbf{K}_{+u}^{(i)}\\ \mathbf{K}_{-\phi}^{(i)} & \mathbf{K}_{-u}^{(i)}\end{bmatrix}\begin{Bmatrix}\hat{\boldsymbol{\phi}}^{(i)}\\ \hat{\mathbf{u}}_0^{(i)}\end{Bmatrix}. \tag{21}$$

It is worthwhile to point out here that in deriving (21) from (20a), the numerical cost is insignificant since the unknown vectors $\hat{\boldsymbol{\psi}}_\pm^{(i)}$ contain only a few unknowns. In fact, numerical results presented in the next section show that two elements on $\Gamma_\pm^{(i)}$ have already produced good results. Substituting expression (21) into (20b) yields

$$[\mathbf{K}_{0\phi}^{(i)} \quad \mathbf{K}_{0u}^{(i)}]\begin{Bmatrix}\hat{\boldsymbol{\phi}}^{(i)}\\ \hat{\mathbf{u}}_0^{(i)}\end{Bmatrix}=\{\mathbf{q}_0^{(i)}\}. \tag{22}$$

It is apparent that eqn (22) gives the equations that are associated with the nodal points on Γ_0^i while expressions (21) represent the contribution of subdomain Ω^i to the boundary nodal points on $\Gamma_\pm^{(i)}$.

The assemblage process of relations (21) and (22) into a system of global "stiffness" (impedance) equations is similar to the *direct stiffness method* in regular FE methods. The construction of the element stiffness matrix and load vector in the regular FE procedure now becomes the construction of an *effective* "stiffness" matrix and the associated "load" vector for the *macro-element* Ω^i. To derive the equations that are associated with points on $\Gamma_\pm^i$, we denote the two macro-elements adjacent to Ω^i as Ω^{i_1} and Ω^{i_2}, respectively (cf. Fig. 2). The transition condition of the pressure derivative (13) may then be expressed, in matrix form, as

$$\{\hat{\boldsymbol{\psi}}_+^{(i)}\}+\{\hat{\boldsymbol{\psi}}_-^{(i_1)}\}=\{0\}, \quad \text{on } \Gamma_+^i, \quad \{\hat{\boldsymbol{\psi}}_-^{(i)}\}+\{\hat{\boldsymbol{\psi}}_+^{(i_2)}\}=\{0\}, \quad \text{on } \Gamma_-^i. \tag{23}$$

Inserting eqn (21) into the above equations yields

$$[\mathbf{K}_{+\phi}^{(i)} \quad \mathbf{K}_{+u}^{(i)}]\begin{Bmatrix}\hat{\boldsymbol{\phi}}^{(i)}\\ \hat{\mathbf{u}}_0^{(i)}\end{Bmatrix}+[\mathbf{K}_{-\phi}^{(i_1)} \quad \mathbf{K}_{-u}^{(i_1)}]\begin{Bmatrix}\hat{\boldsymbol{\phi}}^{(i_1)}\\ \hat{\mathbf{u}}_0^{(i_1)}\end{Bmatrix}=\{\mathbf{q}_+^{(i)}\}+\{\mathbf{q}_-^{(i_1)}\}, \quad \text{on } \Gamma_+^i, \tag{24a}$$

and

$$[\mathbf{K}_{-\phi}^{(i)} \quad \mathbf{K}_{-u}^{(i)}]\begin{Bmatrix}\hat{\boldsymbol{\phi}}^{(i)}\\ \hat{\mathbf{u}}_0^{(i)}\end{Bmatrix}+[\mathbf{K}_{+\phi}^{(i_2)} \quad \mathbf{K}_{+u}^{(i_2)}]\begin{Bmatrix}\hat{\boldsymbol{\phi}}^{(i_2)}\\ \hat{\mathbf{u}}_0^{(i_2)}\end{Bmatrix}=\{\mathbf{q}_-^{(i)}\}+\{\mathbf{q}_+^{(i_2)}\}, \quad \text{on } \Gamma_-^i. \tag{24b}$$

It is obvious that (24a, b) give the equations that are associated with the nodal points on boundaries Γ_+^i and Γ_-^i, and the first terms at both the right- and left-hand sides in eqns (24a, b) represent the contribution of the ith macro-element to the global system of equations. Thus, by combining (22) and (24a, b) and using the standard FE procedure, one arrives at the *effective* macro-element "stiffness" matrix equation for Ω^i:

$$\begin{bmatrix}\mathbf{K}_{0\phi}^{(i)} & \mathbf{K}_{0u}^{(i)}\\ \mathbf{K}_{+\phi}^{(i)} & \mathbf{K}_{+u}^{(i)}\\ \mathbf{K}_{-\phi}^{(i)} & \mathbf{K}_{-u}^{(i)}\end{bmatrix}\begin{Bmatrix}\hat{\boldsymbol{\phi}}^{(i)}\\ \hat{\mathbf{u}}_0^{(i)}\end{Bmatrix}=\begin{Bmatrix}\mathbf{q}_0^{(i)}\\ \mathbf{q}_+^{(i)}\\ \mathbf{q}_-^{(i)}\end{Bmatrix}, \quad \text{or } \mathbf{K}^{(i)}\hat{\mathbf{v}}^{(i)}=\hat{\mathbf{q}}^{(i)}, \tag{25}$$

where $\mathbf{K}^{(i)}$, $\mathbf{q}^{(i)}$ and $\hat{\mathbf{v}}^{(i)}$ represent, respectively, the *effective* "stiffness" (impedance) matrix, the "load" vector and the total nodal unknown vector of macro-element Ω^i. Using the *direct*

stiffness method in FE technique, the "stiffness" matrices $\mathbf{K}^{(i)}$ and "load" vectors $\mathbf{q}^{(i)}$, $i = 1, 2, \ldots, M$, are assembled into a system of global exterior "stiffness" equations:†

$$[\mathbf{K}_\phi \quad \mathbf{K}_{u_0}] \begin{Bmatrix} \hat{\boldsymbol{\phi}} \\ \hat{\mathbf{u}}_0 \end{Bmatrix} = \mathbf{q}, \quad \text{or} \quad K_\phi \hat{\boldsymbol{\phi}} + \mathbf{K}_{u_0} \hat{\mathbf{u}}_0 = \mathbf{q}, \tag{26}$$

where $\hat{\boldsymbol{\phi}}$ is the total pressure unknown vector, whereas $\hat{\mathbf{u}}_0$ represents the nodal displacement vector on the interface Γ. The system of equations (26) consists of N_ϕ linear equations with $N_\phi + N_{u_0}$ unknowns, where N_ϕ is the total number of nodal pressure in $\hat{\phi}$ and N_{u_0} the number of nodal displacement variables in $\hat{\mathbf{u}}_0$. Combining eqns (26) and (11), in view of the fact that $\hat{\mathbf{u}}_0$ and $\hat{\boldsymbol{\phi}}_0$ are, respectively, subsets of $\hat{\mathbf{u}}$ and $\hat{\boldsymbol{\phi}}$, one arrives at the resultant system of linear equations that contains $N_\phi + N_u$ equations with $N_\phi + N_u$ unknowns.

It is worthwhile pointing out that in obtaining $\mathbf{K}^{(i)}$ and $\mathbf{q}^{(i)}$, all the computation is within the subdomain Ω^i. Therefore, one may perform the computation either sequentially or in parallel. Also, as in the standard FE method, only one "stiffness" matrix needs to be constructed for all the macro-elements that have the same geometric configuration and material properties, while the rest may be obtained by duplication.

4. NUMERICAL EXAMPLES

In order to assess the accuracy of our new procedure and to verify that it is valid for all frequencies, we consider problems of two-dimensional thin steel shells submerged in water and subjected to an incident plane wave of amplitude p^0 as in Zeng *et al.* (1992a).

The relative properties, in all cases, are $\rho_e/\rho_f = 7.65$, $c_e/c_f = 3.53$, $\mu_e = 0.3$, where c_e is the velocity of the compressional wave of the elastic shell and μ_e is Poisson's ratio. For the case of circular shells, we take $a/h = 100$, where a is the radius of the shells and h is the thickness of the shell.

Consider first the case where the exterior region Ω_f is decomposed into four macro-elements, i.e. four angular partitions in this case, with varying numbers of elements directly on the fluid–shell interface Γ. Three regular elements will be placed along each ray $\Gamma_\pm^{(i)}$, in addition to the infinite-element, as shown in Fig. 3. Since the infinite element approximations are based on large-distance asymptotic expansions, the purpose of the regular finite elements along radial lines is to serve as a transition between the shell and the region where the asymptotic solution becomes applicable. The size of this transition region obviously depends on the wavenumber.

In all our calculations, three-noded quadratic isoparametric elements are used to represent the boundary Γ^i, the boundary displacement $\mathbf{u}_0^{(i)}$, the pressure $\phi^{(i)}$ and the normal derivative of the pressure $\psi^{(i)}$. The interior elastic shells are modeled with the well-known general shell theory described in Bathe (1982) and Zeng (1992), also using three-noded quadratic isoparametric elements. For simplicity, the number of shell elements used to represent the interior shell structure and that of elements used to represent pressure $\phi^{(i)}$ on the interface Γ are the same.

With these shape functions, all the entries of the individual submatrices in (25) are evaluated by ordinary Gauss–Legendre numerical integration using only four Gaussian points per standard element, except for the diagonal terms of the submatrices containing the singular operator $S^{(i)}$, and $D^{(i)}$ defined by (5a) and (5b), which are integrated after subtracting off singularities. Detailed descriptions of the discretization and integration schemes used in this study may be found in Zeng *et al.* (1992a) and Zeng (1992).

In order to verify the efficiency of the DD-based exterior BIE representation, the integration over the infinite elements is first performed approximately by neglecting contributions beyond a radius of $100/k$, and by subdividing the interval of integration into 16 subintervals, each of which is integrated by a four-point Gauss–Legendre integration. The

† For illustration, $\hat{\mathbf{u}}$ and $\hat{\boldsymbol{\phi}}$ in eqn (26) and also eqn (11) are separated from each other. For numerical implementation, however, the two nodal point vectors must not be separated in order to obtain a blockwise-banded resultant matrix.

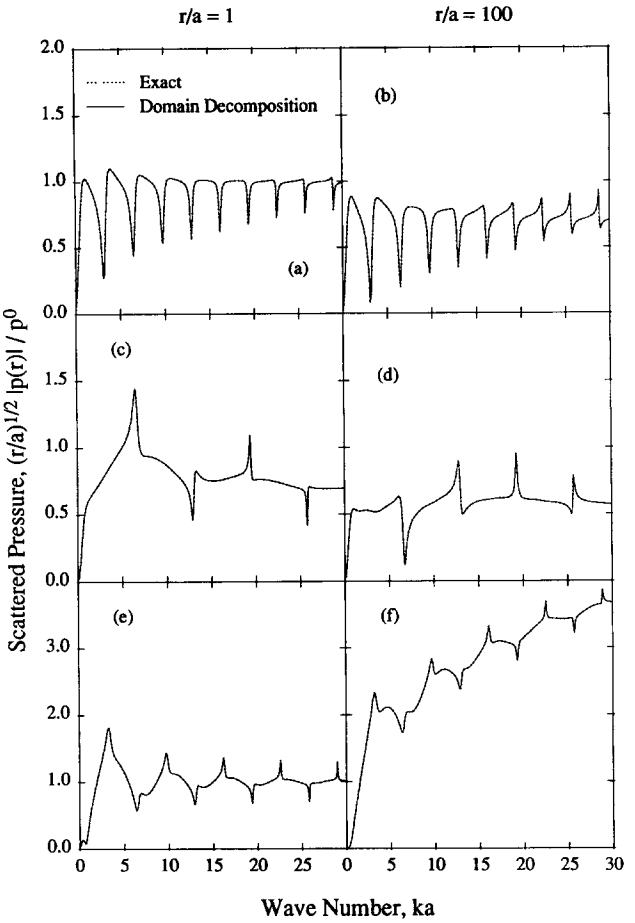

Fig. 4. Normalized amplitude of scattered pressure at various locations as a function of wavenumber. (a) $r/a = 1, \theta = 270°$; (b) $r/a = 100, \theta = 270°$; (c) $r/a = 1, \theta = 0°, 180°$; (d) $r/a = 100, \theta = 0°, 180°$; (e) $r/a = 1, \theta = 90°$; (f) $r/a = 100, \theta = 90°$.

numerical results will show, however, that neglecting the tail end of the rays does not significantly affect the accuracy of the method.

Figure 4 shows the amplitude of the scattered pressure at various locations, both on and outside the shell scatterer, for a wide range of frequencies. Exact solutions obtained from the formulation given by Doolittle and Überall (1965) and Gaunaurd and Brill (1984) are represented by dotted lines, while thin solid lines denote the approximate solutions from the coupled FE and DD-based BIE formulation. The calculations are performed for wavenumbers ka from 0.001 to 30, with a step-size of 0.1, using a varying number of elements on the interface Γ as needed. Thus, while only 16 elements are sufficient at low frequencies, 128 elements are used for $ka = 30$. Up to this frequency, results from the present method and the exact solutions are essentially indistinguishable. By comparing the pressure response profiles shown in Fig. 4 with those obtained from the rigid scattering problem given in Zeng *et al.* (1992a), it can be seen that while the rigid scattering pressure responses are quite smooth with respect to the wavenumber, the responses from the shell–fluid system show greater fluctuations. This phenomenon is obviously due to the two-way interaction between the shell and the exterior fluid. In fact, it has been pointed out in a recent work by Kallivokas *et al.* (1993) that each fluctation or peak corresponds to a physical resonance of the shell–fluid system.

To illustrate how the coupled FE and DD-based BIE approximation for the total and scattered pressures compares with the exact solution over the entire periphery of the shell scatterer and the far field within the fluid, Fig. 5a–f depicts the normalized amplitude of the total pressure on the surface of the scatterer as a function of the angular coordinate θ

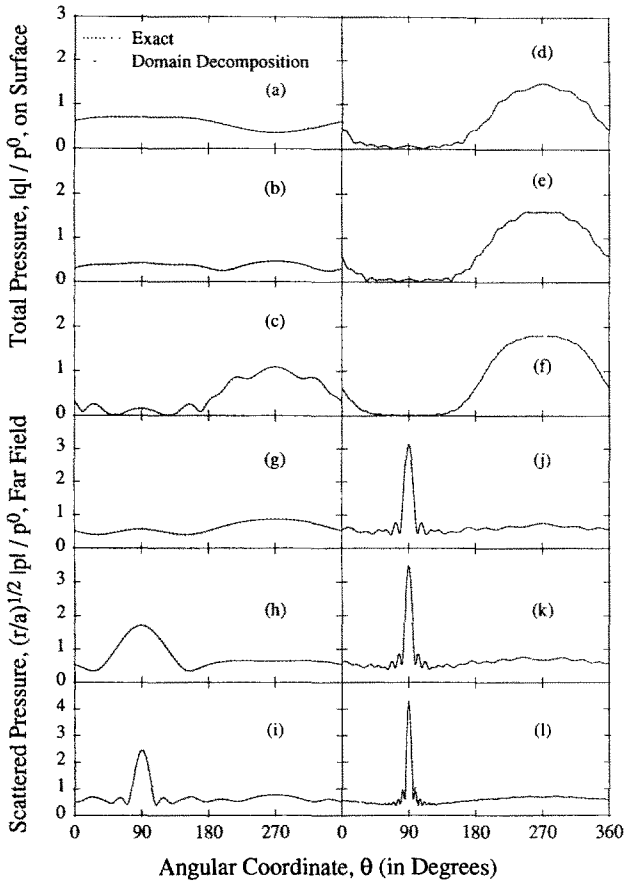

Fig. 5. Normalized amplitude of total pressure. (a–f) On scatterer surface and scattered pressure. (g–l) In far field ($r/a = 100$), for different wavenumbers as a function of angular position. (a, g) $ka = 1$; (b, h) $ka = 2.4048256$; (c, i) $ka = 8.6537278$; (d, j) $ka = 15$; (e, k) $ka = 20$; (f, l) $ka = 30$.

for several wavenumbers, while Fig. 5g–l shows the corresponding scattered pressure at a distance $r/a = 100$. Two of the selected wavenumbers, i.e. $ka = 2.4048256$ and 8.6537379, are taken as the critical frequencies of the associated Helmholtz interior problem. Again, the two solutions practically coincide for all values of θ. These figures illustrate how the normalized amplitude of the total pressure directly on the scatterer tends to 2, as for a flat scatterer, within the bulk of the insonified region (back-scattering) and becomes small, and almost smooth, except for a small high frequency perturbation in the shadow region (forward-scattering), as the wavenumber increases. Apart from this oscillatory behavior in the shadow region, the total pressure on the scatterer practically becomes independent of the wavenumber as the wavenumber becomes large. In the far field, the same general oscillatory and smooth behavior occurs, except that the largest scattering occurs, of course, in front of the shell.

Figure 6 serves to examine how changing the number of macro-elements, i.e. angular partitions in this case, and the number of radial elements on the ray boundaries $\Gamma_{\pm}^{(j)}$ of $\Omega^{(j)}$ affects the accuracy of the solution through two given wavenumbers and for a fixed number of elements on the fluid–shell interface Γ. Figure 6a, b, e, f shows the results from four exterior macro-elements while Fig. 6c, d, g, h shows results from eight macro-elements. The thin solid, thin dashed and thick dashed lines correspond to, respectively, the cases of three, two and one regular radial elements. These results show that the solution is basically insensitive to the number of macro-elements, and that even one regular radial element provides sufficient accuracy. While fewer radial elements mean fewer unknowns, the main advantage of introducing a large number of macro-elements is that one can thus obtain a sparse global matrix that might significantly reduce the computational effort for large scale high frequency fluid–structure interface problems.

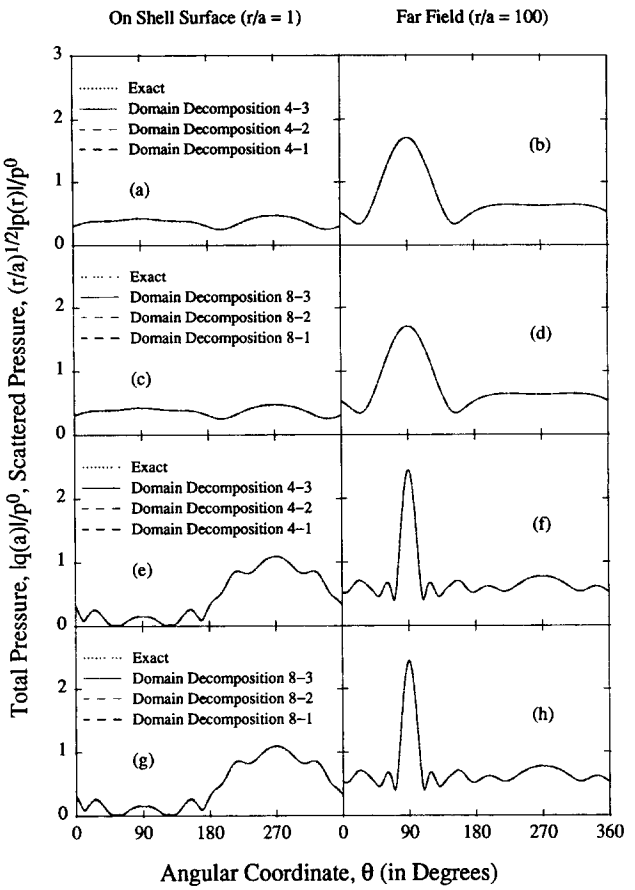

Fig. 6. Effects of no. of macro-elements and no. of standard radial elements on normalized amplitude of total pressure. (a, c, e, g) On shell surface and scattered pressure. (b, d, f, h) In far field ($r/a = 100$), for two critical wavenumbers. (a–d) $ka = 2.4048256$; (e–h) $ka = 8.6537278$, as a function of angular position. (a, b, e, f) Four macro-elements with three, two and one radial elements; (c, d, g, h) eight macro-elements with three, two and one radial elements.

Finally, to evaluate the present method for problems of more complex structural configuration, we consider an elastic shell that has a cross-section consisting of a square with side $2b$ and two semicircles of radius b, $a = 2b$ (cf. Fig. 7e). The thickness of the complex shell is taken as $b/h = 100$. Figure 7 shows the amplitude of total and scattered pressures at various locations. All the results are generated by using eight macro-elements with three regular elements placed along each ray. Since there is no analytical solution for this problem, for comparison, in Fig. 7, we also plot the results generated from the stable coupled FE and *nonlocal* BIE formulation given in Zeng *et al.* (1992b) and Zeng (1992). Again, the calculation is performed for wavenumbers ka from 0.001 to 30. It is clear from Fig. 7 that the results obtained from the present coupled FE and DD-based BIE method and those from the stable coupled FE and *nonlocal* BIE formulation are essentially indistinguishable. Compared with the results from the circular shell cases (cf. Fig. 4), the complex shell pressure responses (cf. Fig. 7) show greater fluctuations. Again, this may be attributed to the two-way interaction between the shell and the exterior fluid (Kallivokas *et al.*, 1993). In fact, even for the circular shell case, there is a large number of resonance wavenumbers. However, the fluctuations near these resonance wavenumbers are so highly localized that an extremely small wavenumber step-size (of the order of 10^{-8}) is needed to actually show the fluctations. Numerical results in Zeng (1992) have shown that as the complexity of the interior structural configuration increases the pressure fluctuation tends to be more violent with respect to the frequency, reflecting the presence of additional modes. To actually understand the complicated pressure response caused by the complex structural configuration, a detailed modal analysis of the structure will be inevitable, which, however, is beyond the scope of this study.

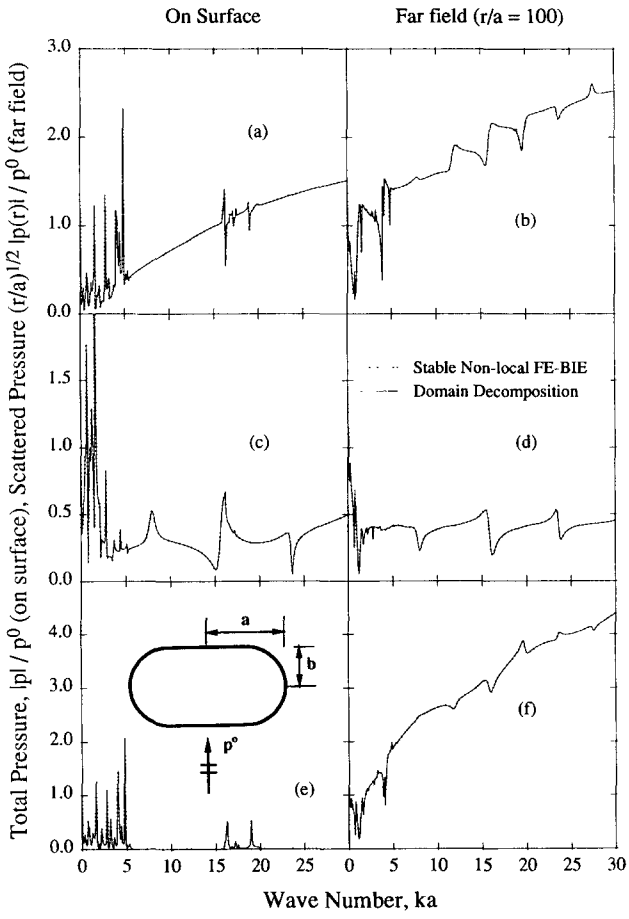

Fig. 7. Normalized amplitude of total (on shell surface) and scattered pressure (in far field) at various locations as a function of wavenumber. (a) $r/b = 1$, $\theta = 270°$; (b) $r/a = 100$, $\theta = 270°$; (c) $r/a = 1$, $\theta = 0°, 180°$; (d) $r/a = 100$, $\theta = 0°, 180°$; (e) $r/b = 1$, $\theta = 90°$; (f) $r/a = 100$, $\theta = 90°$.

5. CONCLUSIONS

The coupled FE and exterior DD-based BIE method presented in this paper combines the BIE method with the sparsity of algebraic systems ordinarily encountered only in domain discretization procedures. The main difference between our approach and the existing *stable* methodologies for fluid–structure interaction problems is, in addition to the blockwise-banded resultant system of linear equations, that the new method uses exclusively single- and double-layer potentials, completely avoiding both the hypersingular operator and the double integrals. Therefore, our method not only avoids the cumbersome treatments of the hypersingular operator in the traditional methods based on collocation but also eliminates the requirement of additional integrations of the double integrals in various variational-based formulations.

From the initial examination of the results of numerical experiments it appears that the coupled FE and DD-based BIE method provides a practical and accurate means for solving time-harmonic fluid–structure interaction problems at all frequencies. The procedure may be formally extended to more general situations, including radiation and scattering problems involving complex deformable inclusions and an elastic exterior. Its main potential advantage over existing coupled FE and BIE methods lies primarily in its ability to generate blockwise-banded algebraic systems of equations. Moreover, by its very design, it also lends itself naturally to implementation on parallel computers. By appropriately selecting the number and location of the subdomains, this method offers the possibility of exploiting optimally the parallel features of a particular parallel architecture.

Acknowledgements—We thank the reviewers for their constructive comments.

REFERENCES

Amini, S. and Harris, P. J. (1990). A comparison between various boundary integral formulations of the exterior acoustic problem. *Comput. Meth. Appl. Mech. Engng* **84,** 59–75.

Bathe, K.-J. (1982). *Finite Element Procedures in Engineering Analysis.* Prentice-Hall, Englewood Cliffs, NJ.

Chien, C. C., Rajiyah, H. and Atluri, S. H. (1990). An effective method for solving the hypersingular integral equations in 3-D acoustics. *J. Acoust. Soc. Am.* **88**(2), 918–937.

Doolittle, R. D. and Überall, H. (1965). Sound scattering by elastic cylindrical shells. *J. Acoust. Soc. Am.* **39**(2), 272–275.

Gaunaurd, G. C. and Brill, D. (1984). Acoustic spectrogram and complex-frequency poles of a resonantly excited elastic tube. *J. Acoust. Soc. Am.* **75**(6), 1680–1693.

Ginsberg, J. H., Chen, P. T. and Pierce, A. D. (1990). Analysis using variational principles of the surface pressure and displacement along axisymmetrically excited disk in a baffle. *J. Acoust. Soc. Am.* **88**(1), 548–559.

Givoli, D. (1991). Non-reflecting boundary conditions. *J. Comput. Phys.* **94,** 1–29.

Hughes, T. J. R. (1987). *The Finite Element Method, Linear Static and Dynamic Finite Element Analysis.* Prentice-Hall, Englewood Cliffs, NJ.

Jeans, R. A. and Mathews, I. C. (1990). Solution of fluid–structure interaction problems using a coupled finite element and variational boundary element technique. *J. Acoust. Soc. Am.* **88**(5), 2459–2466.

Kagawa, Y., Yamabuchi, T. and Kitagami, S. (1983). Infinite boundary element and its application to combined finite-boundary element technique for unbounded field problem. In *Boundary Element Methods in Engineering* (Edited by C. A. Brebbia), pp. 1017–1026. Springer-Verlag, Berlin.

Kallivokas, L. F., Zeng, X. and Bielak, J. (1994). Stable localized BEM–FEM for fluid–structure interaction. Submitted to *J. Acoust. Soc. Am.*

Krishnasamy, G., Schmerr, L. W., Rudolphi, T. J. and Rizzo, F. J. (1990). Hypersingular boundary integral equations: some applications in acoustic and elastic wave scattering. *J. Appl. Mech.* **57**(2), 404–414.

Lamb, H. (1945). *Hydrodynamics*, 6th Edn, see article 290. Dover, New York.

Schenck, H. A. (1968). Improved integral formulation for acoustic radiation problems. *J. Acoust. Soc. Am.* **44**(1), 41–58.

Seybert, A. F., Soenkarko, B., Rizzo, F. J. and Shippy, D. J. (1985). An advanced computational method for radiation and scattering of acoustic waves in three dimensions. *J. Acoust. Soc. Am.* **77**(2), 362–367.

Seybert, A. F., Wu, T. W. and Wu, X. F. (1988). Radiation and scattering from elastic solid and shell using the BEM. *J. Acoust. Soc. Am.* **84**(5), 1906–1912.

Zeng, X. (1992). Stable symmetric FEM–BEM coupling method for fluid–structure interface problems with applications. Ph.D. Thesis, Dept. of Civil Engineering, Carnegie Mellon University, Pittsburgh, PA.

Zeng, X. and Bielak, J. (1994). Exterior stable domain decomposition integral equation method for scattering problems. (To appear.) *Int. J. Numer. Meth. Engng.*

Zeng, X., Kallivokas, L. and Bielak, J. (1992a). Stable localized symmetric integral equation method for acoustic scattering problems. *J. Acoust. Soc. Am.* **91**(5), 2510–2518.

Zeng, X., Bielak, J. and MacCamy, R. C. (1992b). Unified symmetric finite element and boundary integral variational coupling method for fluid–structure interaction. *Numer. Meth. Partial Diff. Eqns* **8,** 451–467.

Zeng, X., Bielak, J. and MacCamy, R. C. (1992c). Stable variational coupling method for fluid–structure interaction in semi-infinite media. *ASME J. Vibr. Acoust.* **114,** 387–396.

Zienkiewicz, O. C., Bando, K., Bettes, P., Emson, C. and Chiam, C. (1985). Mapped infinite elements for exterior wave problems. *Int. J. Numer. Meth. Engng* **21,** 1229–1251.